

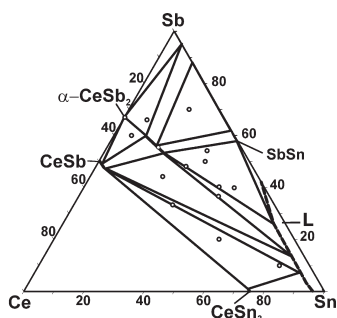
Abstracted/indexed in BioEngineering Abstracts, Chemical Abstracts, Coal Abstracts, Current Contents/Physics, Chemical, & Earth Sciences, Engineering Index, Research Alert, SCISEARCH, Science Abstracts, and Science Citation Index. Also covered in the abstract and citation database SCOPUS<sup>®</sup>. Full text available on ScienceDirect<sup>®</sup>.

### Regular Articles

#### Phase equilibria in systems Ce–M–Sb ( $M = \text{Si, Ge, Sn}$ ) and superstructure $\text{Ce}_{12}\text{Ge}_{9-x}\text{Sb}_{23+x}$ ( $x = 3.8 \pm 0.1$ )

Navida Nasir, Andriy Grytsiv, Peter Rogl, Adriana Saccone and Gerald Giester

Page 645



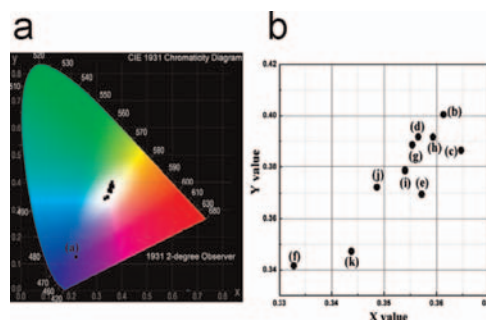
Phase relations in the ternary systems Ce–M–Sb ( $M = \text{Si, Ge, Sn}$ ) in composition regions  $\text{CeSb}_2$ –Sb–M have been studied by optical and electron microscopy, XRD and EPMA on as cast alloys and specimens annealed in the temperature region 200–850 °C.

### Regular Articles—Continued

#### White light emission from $\text{Tm}^{3+}/\text{Dy}^{3+}$ co-doped oxyfluoride germanate glasses under UV light excitation

G. Lakshminarayana, Hucheng Yang and Jianrong Qiu

Page 669

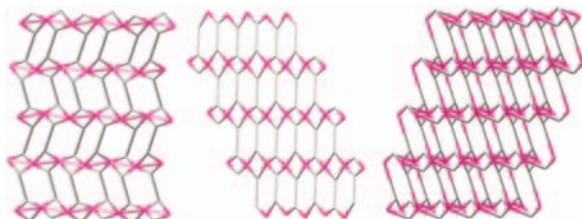


A combination of blue, yellow and red emissions has emerged from  $\text{Tm}^{3+}/\text{Dy}^{3+}$  co-doped glasses, which allows the observation of bright white light and makes them as excellent candidates applicable in the solid-state multi-colour three-dimensional display.

#### Synthesis, crystal structure and photoluminescent properties of four lanthanide 5-nitroisophthalate coordination polymers

Yan Huang, Bing Yan and Min Shao

Page 657

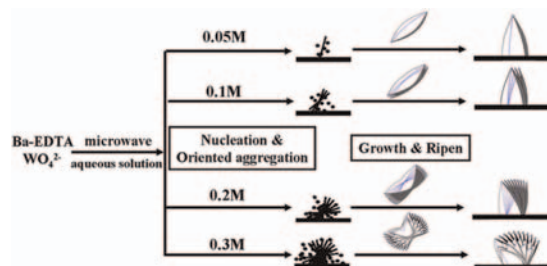


Four lanthanide 5-nitroisophthalate coordination polymers have been hydrothermally prepared and present different structures and thermal stabilities and photoluminescence properties.

#### Fabrication and morphology control of $\text{BaWO}_4$ thin films by microwave assisted chemical bath deposition

Rui Wang, Chen Liu, Jia Zeng, KunWei Li and Hao Wang

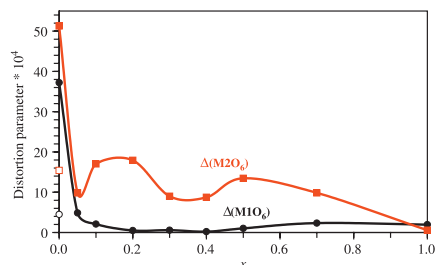
Page 677



Highly crystallized  $\text{BaWO}_4$  thin films with controllable morphologies have been synthesized via mild microwave assisted chemical bath deposition. The oriented aggregation mechanism has been proposed as the possible formation mechanism of specific films.

## Evolution of structural distortions in solid solutions between BiMnO<sub>3</sub> and BiScO<sub>3</sub>

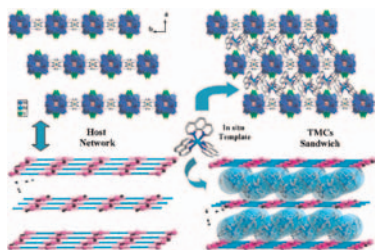
Alexei A. Belik, Kenichi Kato and qEiji Takayama-Muromachi  
Page 685



Compositional dependence of octahedral distortion parameters  $\Delta(M1O_6)$  and  $\Delta(M2O_6)$  in solid solutions  $BiMn_{1-x}Sc_xO_3$  at 300 K.

## Two new transition-metal complexes (TMCs)-templated three-dimensional supramolecular networks based on tungstovanadophosphates

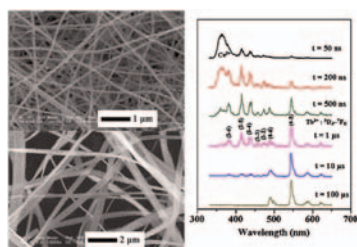
Yu-Kun Lu, Xiao-Bing Cui, Ya-Bing Liu, Qing-Feng Yang, Shu-Yun Shi, Ji-Qing Xu and Tie-Gang Wang  
page 690



The structures of  $[Ni(phen)_3][Ni(en)_3][Ni(en)_2(H_2O)_2][Ni(en)_2]_{0.5}[PW^{VI}_7W^{V}_2V^{IV}_3O_{40}(V^{IV}O)_2] \cdot 6H_2O$  (1) and  $[Ni(phen)_3]_2[Ni(en)_2]Na[PW^{VI}_7W^{V}_2V^{IV}_3O_{40}(V^{IV}O)_2] \cdot 8H_2O$  (2) exhibit interesting 3D supramolecular networks constructed by bicapped Keggin heteropolyanions and the *in situ* templates transition metal complexes.

## Preparation and luminescence properties of Ce<sup>3+</sup> and/or Tb<sup>3+</sup> doped LaPO<sub>4</sub> nanofibers and microbelts by electrospinning

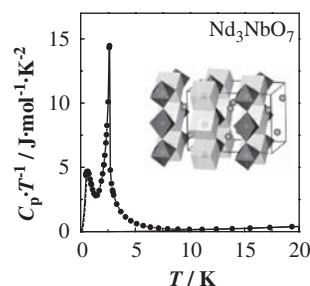
Zhiyao Hou, Lili Wang, Hongzhou Lian, Ruitao Chai, Cuimiao Zhang, Ziyong Cheng and Jun Lin  
Page 698



Ce<sup>3+</sup> and/or Tb<sup>3+</sup> LaPO<sub>4</sub> nanofibers and microbelts have been prepared by electrospinning. A systematic study on the optical properties of LaPO<sub>4</sub>:Ce<sup>3+</sup>, Tb<sup>3+</sup> samples has shown that they are good green-emitting phosphors in fluorescent lamps and field emission displays. The energy transfer process from Ce<sup>3+</sup> to Tb<sup>3+</sup> in LaPO<sub>4</sub>:Ce<sup>3+</sup>, Tb<sup>3+</sup> nanofibers is further studied by the time-resolved emission spectra.

## Crystal structures and magnetic properties of fluorite-related oxides Ln<sub>3</sub>NbO<sub>7</sub> (Ln = lanthanides)

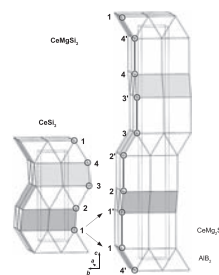
Yoshihiro Doi, Yuka Harada and Yukio Hinatsu  
Page 709



Ternary oxides  $Ln_3NbO_7$  ( $Ln$  = lanthanides) have the fluorite-related structures with space group  $Pnma$  ( $Ln$  = La, Pr, Nd),  $C222_1$  ( $Ln$  = Sm–Tb), or  $Fm-3m$  ( $Ln$  = Dy–Lu). In them,  $Nd_3NbO_7$  and  $Tb_3NbO_7$  show “two-step” antiferromagnetic transitions due to the long-range antiferromagnetic ordering of  $Ln$  ions in different crystallographic sites.

## Synthesis and crystal structure of RMgSi<sub>2</sub> compounds (R = La, Ce, Pr, Nd), a particular example of linear intergrowth

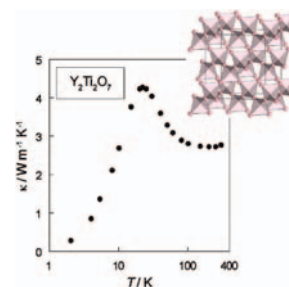
F. Wrubl, M. Pani, P. Manfrinetti and P. Rogl  
Page 716



The new crystal structure of  $CeMgSi_2$  can be formally built up by alternating along the  $z$  direction, four  $CeMg_2Si_2$ -type  $CeMg_2Si_2$  slabs with four  $AlB_2$ -type  $CeSi_2$  slabs, one after the other. A close symmetry relationship holds between the  $ThSi_2$  and  $CeMgSi_2$  structure types, as shown in the figure.

## Thermal properties of the pyrochlore, Y<sub>2</sub>Ti<sub>2</sub>O<sub>7</sub>

Michel B. Johnson, David D. James, Alex Bourque, Hanna A. Dabkowska, Bruce D. Gaulin and Mary Anne White  
Page 725

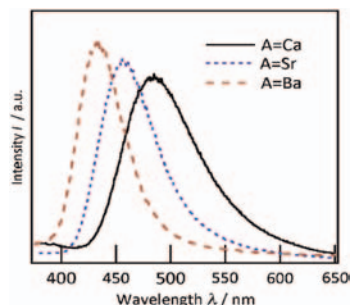


The thermal conductivity and heat capacity of high-purity single crystals of yttrium titanate,  $Y_2Ti_2O_7$ , have been determined in the range  $2 K \leq T \leq 300 K$ . The thermal conductivity shows a peak at ca.  $\theta_D/50$ , characteristic of a highly purified crystal in which the phonon mean free path is about  $10 \mu m$  in the defect/boundary low-temperature limit.

## Structural investigation of $\text{Eu}^{2+}$ emissions from alkaline earth zirconium phosphate

Masaaki Hirayama, Noriyuki Sonoyama, Atsuo Yamada and Ryoji Kanno

Page 730

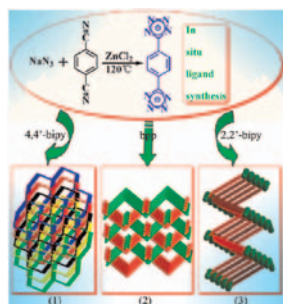


$\text{Eu}^{2+}$  doped NASICON structured  $\text{A}_{0.5}\text{Zr}_2(\text{PO}_4)_3$  ( $\text{A} = \text{Ca}, \text{Sr}, \text{Ba}$ ) showed the blue and blue-green colored emissions attributed to  $4f^65d^1-4f^7$  transitions. The photoluminescent properties are discussed in terms of crystal field strength and nephelauxetic effect using powder X-ray Rietveld analysis.

## Entangled zinc-ditetrazolate frameworks involving in situ ligand synthesis and topological modulation by various secondary N-donor ligands

Yun-Wu Li, Wei-Lin Chen, Yong-Hui Wang, Yang-Guang Li and En-Bo Wang

Page 736

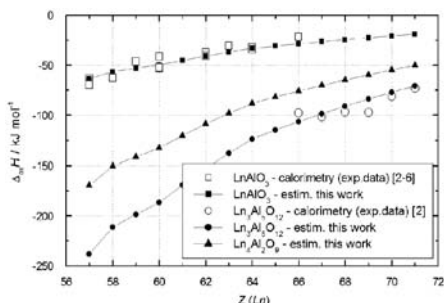


Three new entangled frameworks were prepared by an in situ ditetrazolate-ligand synthesis system assisted with various auxiliary N-donor ligands. The entangled structures can be modulated by different secondary ligands.

## A method for the estimation of the enthalpy of formation of mixed oxides in $\text{Al}_2\text{O}_3\text{-Ln}_2\text{O}_3$ systems

P. Voňka and J. Leitner

Page 744

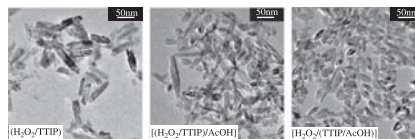


Enthalpy of formation of Ln-Al-O oxides from the constituent binary ones.

## Morphological and phase evolution of $\text{TiO}_2$ nanocrystals prepared from peroxotitanate complex aqueous solution: Influence of acetic acid

Jeong Ah Chang, Muga Vithal, In Chan Baek and Sang Il Seok

Page 749



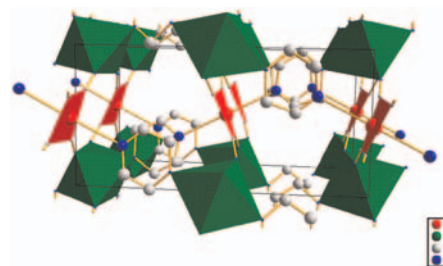
The morphology of  $\text{TiO}_2$  depends on the sequence of addition of AcOH and  $\text{H}_2\text{O}_2$  from the system of titanium isopropoxide and acetic acid (AcOH) in the presence of  $\text{H}_2\text{O}_2$ .

## Unique coordination of pyrazine in $T[\text{Ni}(\text{CN})_4] \cdot 2\text{pyz}$ with $T = \text{Mn}, \text{Zn}, \text{Cd}$

A.A. Lemus-Santana, J. Rodríguez-Hernández,

L.F. del Castillo, M. Basterrechea and E. Reguera

Page 757



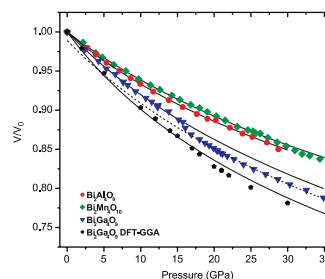
Framework for  $T[\text{Ni}(\text{CN})_4] \cdot 2\text{pyz}$  with  $T = \text{Mn}, \text{Zn}, \text{Cd}$ .

## High-pressure behavior of the ternary bismuth oxides $\text{Bi}_2\text{Al}_4\text{O}_9$ , $\text{Bi}_2\text{Ga}_4\text{O}_9$ and $\text{Bi}_2\text{Mn}_4\text{O}_{10}$

Laura López-de-la-Torre, Alexandra Friedrich, Erick A. Juarez-Arellano, Björn Winkler, Dan J. Wilson,

Lkhamsuren Bayarjargal, Michael Hanfland, Manfred Burianek, Manfred Mühlberg and Hartmut Schneider

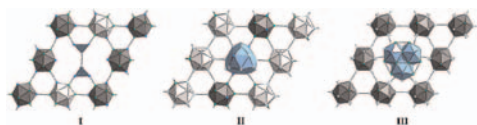
Page 767



The influence of cation substitution on the high-pressure behavior of ternary bismuth oxides was investigated by powder X-ray diffraction using the diamond anvil cell technique. While  $\text{Bi}_2\text{Ga}_4\text{O}_9$  shows a reversible phase transition at approximately 16 GPa,  $\text{Bi}_2\text{Al}_4\text{O}_9$  and  $\text{Bi}_2\text{Mn}_4\text{O}_{10}$  are structurally stable up to 29 and 35 GPa, respectively. Complementary density functional theory-based model calculations were performed on  $\text{Bi}_2\text{Ga}_4\text{O}_9$ .

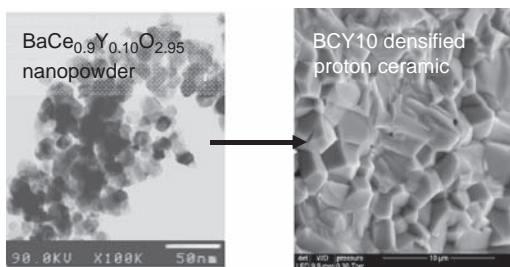
Continued

**Networks of icosahedra in the sodium–zinc–stannides**  
 $\text{Na}_{16}\text{Zn}_{13.54}\text{Sn}_{13.46(5)}$ ,  $\text{Na}_{22}\text{Zn}_{20}\text{Sn}_{19(1)}$ , and  $\text{Na}_{34}\text{Zn}_{66}\text{Sn}_{38(1)}$   
 Sung-Jin Kim and Thomas F. Fässler  
 Page 778



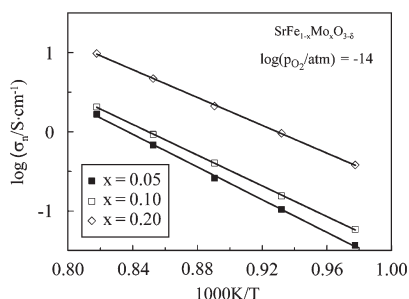
Three new compounds  $\text{Na}_{16}\text{Zn}_{13.54}\text{Sn}_{13.46(5)}$  (**I**),  $\text{Na}_{22}\text{Zn}_{20}\text{Sn}_{19(1)}$  (**II**), and  $\text{Na}_{34}\text{Zn}_{66}\text{Sn}_{38(1)}$  (**III**) were obtained from the elements and were characterized by single-crystal X-ray diffraction. Their structures have in common Kagome layers of  $\{\text{Zn}_{12-x}\text{Sn}_x\}$  icosahedra. Additional building units, such as triangles, 15-atom spacer, and triply fused icosahedra fill the structures of **I**, **II**, and **III**, respectively. The structures and the electron requirements are discussed.

**New synthesis of nanopowders of proton conducting materials. A route to densified proton ceramics**  
 Zohreh Khani, Mélanie Taillades-Jacquín, Gilles Taillades, Mathieu Marrony, Deborah J. Jones and Jacques Rozière  
 Page 790



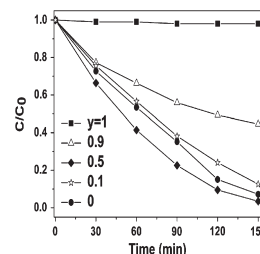
Low temperature hydrogelation and micro-emulsion routes have been developed for the preparation of rare earth doped barium and zirconium cerates in the form of nanoparticulate powders for use after densification as ceramic membranes for a proton ceramic fuel cell.

**Structural features, nonstoichiometry and high-temperature transport in  $\text{SrFe}_{1-x}\text{Mo}_x\text{O}_{3-\delta}$**   
 A.A. Markov, O.A. Savinskaya, M.V. Patrakeevev, A.P. Nemudry, I.A. Leonidov, Yu.T. Pavlyukhin, A.V. Ishchenko and V.L. Kozhevnikov  
 Page 799



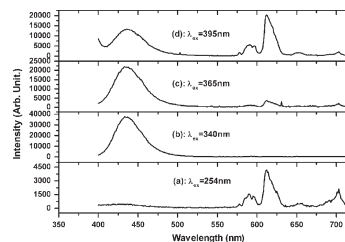
An electron conductivity in  $\text{SrFe}_{1-x}\text{Mo}_x\text{O}_{3-\delta}$  in reducing conditions.

**Preparation and photocatalytic activity of high-efficiency visible-light-responsive photocatalyst  $\text{SnS}_x/\text{TiO}_2$**   
 Chongyin Yang, Wendeng Wang, Zhichao Shan and Fuqiang Huang  
 Page 807



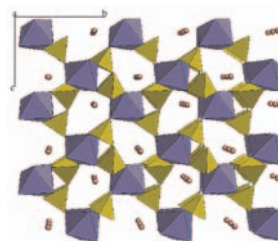
Visible-light-responsive composite photocatalysts  $\text{SnS}_2/\text{TiO}_2$  and  $\text{SnS}/\text{TiO}_2$  with different mass ratios were prepared by in-situ synthesis technology in solution with commercial  $\text{TiO}_2$ . The photocatalysts  $\text{SnS}_x$  ( $x = 1, 2$ ) and  $\text{SnS}_x/\text{TiO}_2$  possess excellent photocatalytic activities. The greatly enhanced photocatalytic activity of the  $\text{SnS}_x/\text{TiO}_2$  composites was mainly attributed to the matching band potentials and efficient charge transfer and separation at the tight-bonding interface between  $\text{SnS}_x$  and  $\text{TiO}_2$ .

**Electronic properties and rare-earth ions photoluminescence behaviors in borosilicate:  $\text{SrB}_2\text{Si}_2\text{O}_8$**   
 Yuhua Wang, Zhiya Zhang, Jiachi Zhang and Yanghua Lu  
 Page 813



The emissions of  $\text{SrB}_2\text{Si}_2\text{O}_8:\text{Eu}$  prepared in air can be switched between the red (611 nm) and the blue (440 nm) by different excitations: under 254 nm excitation the  $\text{Eu}^{3+}$  red emission is dominant while under 365 nm excitation the  $\text{Eu}^{2+}$  blue emission prevails at the emission spectra; when excited by 340 nm it emits almost the pure blue; and when excited by 395 nm the two emissions present nearly equivalent intensity.

**Crystal structure, magnetic and infrared spectroscopy studies of the  $\text{LiCr}_y\text{Fe}_{1-y}\text{P}_2\text{O}_7$  solid solution**  
 Hssain Bih, Ismael Saadoun, Helmut Ehrenberg and Hartmut Fues  
 Page 821

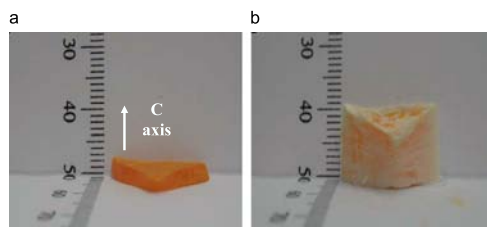


Crystal structure of  $\text{LiCr}_y\text{Fe}_{1-y}\text{P}_2\text{O}_7$  diphosphates, view along the 'a' axis. Red circles denote the lithium atoms. For interpretation of this figure legend, the reader is referred to the web version of this article.

## Photoluminescence and Raman spectroscopy studies on polyaniline/PbI<sub>2</sub> composite

M. Baibarac, I. Baltog and S. Lefrant

Page 827

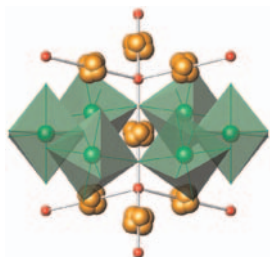


Experimental illustration of the extending along the *c* axis of a PbI<sub>2</sub> single crystal by an intercalation process. In (a) is shown a crystal slide cleaved from a Bridgman-grown PbI<sub>2</sub> crystal ingot and in (b) the same sample intercalated with pyridine obtained after an exposure for 24 h in a saturated atmosphere of pyridine.

## Synthesis and structural studies of lanthanide substituted bismuth–titanium pyrochlores

Jimmy Ting, Brendan J. Kennedy, Ray L. Withers and Maxim Avdeev

Page 836

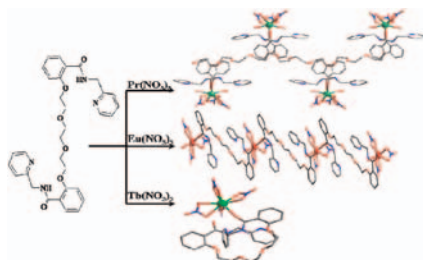


The pyrochlore phase formed during the synthesis of the ferroelectric oxides Bi<sub>4-x</sub>Ln<sub>x</sub>Ti<sub>3</sub>O<sub>12</sub> is shown to be Bi<sub>2/3</sub>Ln<sub>4/3</sub>Ti<sub>2</sub>O<sub>7</sub>. This is found to be stable only for Ln<sup>3+</sup> cations smaller than Sm<sup>3+</sup>. Displacive disorder of the Bi and Ln cations is observed.

## Structure variation and luminescence properties of lanthanide complexes with 1,9-bis [2-(2'-picolylaminoformyl)-1,4,7,9-tetraoxadecane

Xue-Qin Song, Zhi-Peng Zang, Wei-Sheng Liu and Yu-Jie Zhang

Page 841

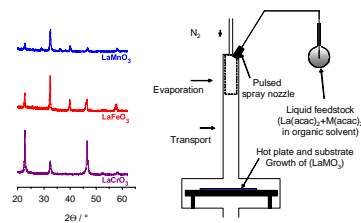


Structure variation and luminescence properties of lanthanide complexes with 1,9-bis [2-(2'-picolylaminoformyl)-1,4,7,9-tetraoxadecane.

## Chemical vapor deposition and electric characterization of perovskite oxides LaMO<sub>3</sub> (M = Co, Fe, Cr and Mn) thin films

Patrick Herve Tchoua Ngamou and Naoufal Bahlwane

Page 849



We report a single step deposition of perovskite thin films LaMO<sub>3</sub> (M: Co, Mn, Cr, Fe) using pulsed spray evaporation chemical vapor deposition. Electrical and thermopower properties, similar to these of bulk materials, could promote the development of modern thermoelectric devices based on thin films technology.

## Synthesis, crystal structure and optical properties of an indium phosphate K<sub>3</sub>In<sub>3</sub>P<sub>4</sub>O<sub>16</sub>

S.-L. Yang, H. Zhang, Z. Xie, D. Zhao, W.-L. Zhang and W.-D. Cheng

Page 855

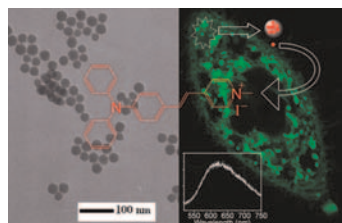


A new indium phosphate crystal, K<sub>3</sub>In<sub>3</sub>P<sub>4</sub>O<sub>16</sub>, was synthesized by a high-temperature solid-state reaction with space group *P2<sub>1</sub>/n*. It possesses three-dimensional [In<sub>3</sub>(PO<sub>4</sub>)<sub>4</sub>]<sup>3-</sup> anionic frameworks built by InO<sub>6</sub> octahedra, InO<sub>7</sub> decahedra and PO<sub>4</sub> tetrahedra, and with tunnels occupied by K1 and K2 running along the *a*-axis, while K3 cations are located in cavities of the structure.

## Uniform silica nanoparticles encapsulating two-photon absorbing fluorescent dye

Wei-Bing Wu, Chang Liu, Ming-Liang Wang, Wei Huang, Sheng-Rui Zhou, Wei Jiang, Yue-Ming Sun, Yi-Ping Cui and Chun-Xin Xu

Page 862

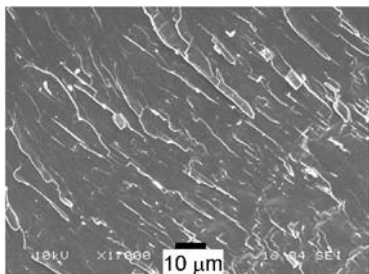


Water-soluble silica NPs doped with a two-photon absorbing zwitterionic hemicyanine dye were prepared. They were found of enhanced one-photon and two-photon excited fluorescence compared to free dye solutions. Images from two-photon laser scanning microscopy demonstrate that the dye-doped silica NPs can be actively uptaken by Hela cells.

Continued

**The influence of co-doping Ag and Sb on microstructure and thermoelectric properties of PbTe prepared by combining hydrothermal synthesis and melting**

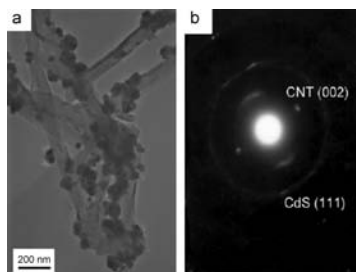
H. Li, K.F. Cai, H.F. Wang, L. Wang, J.L. Yin and C.W. Zhou  
Page 869



SEM image of the fracture surface of an AgPb<sub>18</sub>SbTe<sub>20</sub> material prepared by combining hydrothermal synthesis and melting. The material has a ZT value of about 0.94 at 723 K.

**A simple route to synthesize carbon-nanotube/cadmium-sulfide hybrid heterostructures and their optical properties**

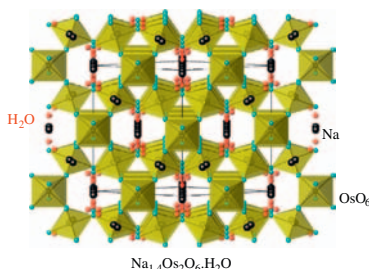
Yongbin Zhao, Haijing Liu, Feng Wang, Jingjun Liu, Ki Chul Park and Morinobu Endo  
Page 875



Transmission electron micrograph observation and electron diffraction pattern analysis of MWCNT/CdS heterostructures, which show that CdS nanoparticles with cubic CdS phase are deposited on the surface of MWCNTs.

**Magnetic and charge transport properties of the Na-based Os oxide pyrochlore**

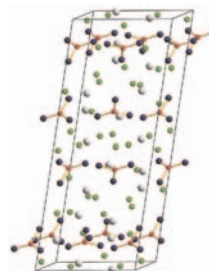
Y.G. Shi, A.A. Belik, M. Tachibana, M. Tanaka, Y. Katsuya, K. Kobayashi, K. Yamaura and E. Takayama-Muromachi  
Page 881



Crystal structure of the Na-based Os oxide pyrochlore Na<sub>1.4</sub>Os<sub>2</sub>O<sub>6</sub>·H<sub>2</sub>O.

**High-pressure synthesis, crystal structure, and structural relationship of the first ytterbium fluoride borate**

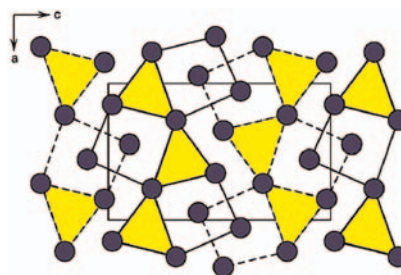
Yb<sub>5</sub>(BO<sub>3</sub>)<sub>2</sub>F<sub>9</sub>  
Almut Haberer and Hubert Huppertz  
Page 888



High-pressure/high-temperature synthesis (multi-anvil technique) led to the first ytterbium fluoride borate Yb<sub>5</sub>(BO<sub>3</sub>)<sub>2</sub>F<sub>9</sub>, built up from isolated BO<sub>3</sub>-groups. The compound shows structural relations to the known rare-earth fluoride borates RE<sub>3</sub>(BO<sub>3</sub>)<sub>2</sub>F<sub>3</sub> (RE = Sm, Eu, Gd) and Gd<sub>2</sub>(BO<sub>3</sub>)F<sub>3</sub>.

**The crystal structure of Hf<sub>1.5+δ</sub>Nb<sub>1.5-δ</sub>As and structure-composition relations in the section Hf<sub>3</sub>As-Nb<sub>3</sub>As**

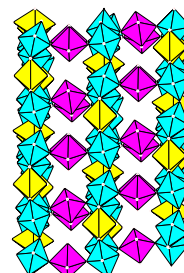
Piotr Warczok, Igor Chumak and Klaus W. Richter  
Page 896



Hf<sub>1.5+δ</sub>Nb<sub>1.5-δ</sub>As with a new structure type (space group *Pnma*; lattice parameters  $a = 7.142(2)$  Å,  $b = 3.583(2)$  Å,  $c = 11.640(2)$  Å) was synthesized. Phase relations, energies and partial ordering in the section Hf<sub>3</sub>As-Nb<sub>3</sub>As were studied by first principle DFT calculations and thermodynamic modelling.

**[Ni(H<sub>2</sub>O)<sub>4</sub>]<sub>3</sub>[U(OH,H<sub>2</sub>O)(UO<sub>2</sub>)<sub>8</sub>O<sub>12</sub>(OH)<sub>3</sub>], crystal structure and comparison with uranium minerals with U<sub>3</sub>O<sub>8</sub>-type sheets**

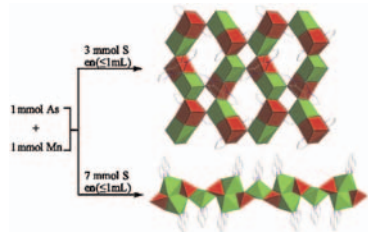
Murielle Rivenet, Nicolas Vigier, Pascal Roussel and Francis Abraham  
Page 905



The framework of [Ni(H<sub>2</sub>O)<sub>4</sub>]<sub>3</sub>[U(OH,H<sub>2</sub>O)(UO<sub>2</sub>)<sub>8</sub>O<sub>12</sub>(OH)<sub>3</sub>] built from uranium polyhedra sheets pillared by Ni-centered octahedra.

**Syntheses, crystal structures, and characterization of As(III) and As(V) thioarsenates,  $[\text{Mn}_2(\text{phen})(\text{As}_2^{\text{III}}\text{S}_5)]_n$  and  $[\text{Mn}_3(\text{phen})_3(\text{As}^{\text{V}}\text{S}_4)_2]_n \cdot n\text{H}_2\text{O}$**

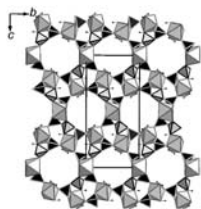
Xin Wang, Tian-Lu Sheng, Sheng-Min Hu, Rui-Biao Fu, Jian-Shan Chen and Xin-Tao Wu  
**Page 913**



Two manganese As(III) and As(V) thioarsenates, namely,  $[\text{Mn}_2(\text{phen})(\text{As}_2^{\text{III}}\text{S}_5)]_n$  (**1**) (top structure) and  $[\text{Mn}_3(\text{phen})_3(\text{As}^{\text{V}}\text{S}_4)_2]_n \cdot n\text{H}_2\text{O}$  (**2**) (bottom structure), have been isolated under hydrothermal conditions. Compound **1** is a 2D layer of (6,3) topology, while that of **2** is a 1D chain structure. The oxidation-state of arsenic might be related to the molar ratio of the reactants. They are both characterized by IR, elemental analysis, X-ray powder diffraction, and EDS. The thermogravimetric analysis and magnetism of **1** and **2** are discussed. Both the compounds are semiconductors.

**Hydrothermal synthesis, crystal structure, and magnetic properties of a novel organo-templated iron(III) borophosphate:  $(\text{C}_3\text{H}_{12}\text{N}_2)\text{Fe}^{\text{III}}_6(\text{H}_2\text{O})_4[\text{B}_4\text{P}_8\text{O}_{32}(\text{OH})_8]$**

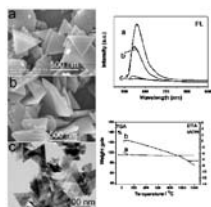
Ya-Xi Huang, Walter Schnelle, Hui Zhang, Horst Borrmann and Rüdiger Kniep  
**Page 920**



The complex inorganic open-framework of  $(\text{C}_3\text{H}_{12}\text{N}_2)\text{Fe}^{\text{III}}_6(\text{H}_2\text{O})_4[\text{B}_4\text{P}_8\text{O}_{32}(\text{OH})_8]$  consists of borophosphate trimers and iron(III) coordination octahedra arranged to form channels with ten-membered ring apertures in which the organic 1,3-diaminopropane cations are located.

**Synthesis of highly crystalline rhombohedral BN triangular nanoplates via a convenient solid state reaction**

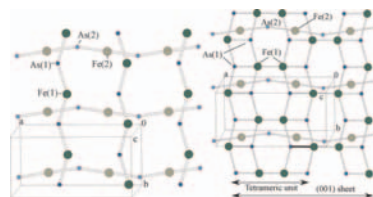
Keyan Bao, Fengyang Yu, Liang Shi, Shuzhen Liu, Xiaobo Hu, Jie Cao and Yitai Qian  
**Page 925**



Rhombohedral BN triangular nanoplates were synthesized at 600 °C. The products exhibit excellent luminescence, thermal stability and anti-oxidation properties; they are expected to become good candidates for optical and optoelectronic devices.

**Mild hydrothermal synthesis, crystal structure, thermal behavior, spectroscopic and magnetic properties of the  $(\text{NH}_4)[\text{Fe}(\text{AsO}_4)_{1-x}(\text{PO}_4)_x\text{F}]$  ( $x = 0.3, 0.6, 0.8$ ) series.**

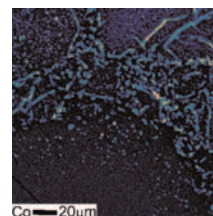
**Thermal transformation of  $(\text{NH}_4)[\text{Fe}(\text{AsO}_4)_{0.7}(\text{PO}_4)_{0.3}\text{F}]$  into the textural porous orthorhombic  $\text{Fe}(\text{AsO}_4)_{0.7}(\text{PO}_4)_{0.3}$**   
 Teresa Berrocal, José L. Mesa, José L. Pizarro, Begoña Bazán, Luis Lezama, María I. Arriortua and Teófilo Rojo  
**Page 932**



The relationship between the  $|100|$  and  $|010|$  chains in  $(\text{NH}_4)[\text{Fe}(\text{AsO}_4)_{1-x}(\text{PO}_4)_x\text{F}]$  left and the  $|100|$  chains and the (001) sheets in  $\text{Fe}(\text{AsO}_4)_{0.7}(\text{PO}_4)_{0.3}$ .

**The solubility of Co in  $\text{TiO}_2$  anatase and rutile and its effect on the magnetic properties**

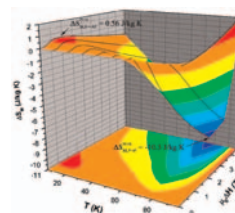
Meike Fleischhammer, Martin Panthöfer and Wolfgang Tremel  
**Page 942**



Co-doped anatase and rutile bulk-samples prepared by the sol-gel technique are paramagnetic at room-temperature. Further annealing in  $\text{Ar}/\text{H}_2$  gas results in a ferromagnetic behavior. X-ray diffraction and electron-microscope (SEM, BSE) studies reveal for low doping levels  $<4\%$  the formation of Co-doped rutile samples and of  $\text{CoTiO}_3$  as a new phase.  $\text{Co}_3\text{O}_4$  is found in anatase samples with Co doping levels  $\geq 4\%$ . The observed Co oxides are reduced by  $\text{Ar}/\text{H}_2$  to Co metal. The room-temperature ferromagnetism can be traced back to a segregation of metallic Co.

**Metamagnetic transition in the 75 K antiferromagnet  $\text{Gd}_4\text{Co}_2\text{Mg}_3$**

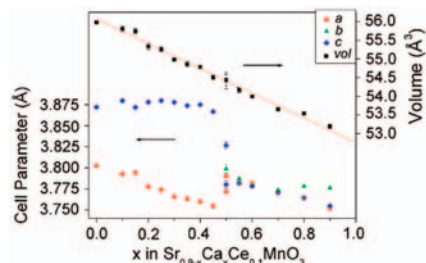
S. Gorsse, B. Chevalier, S. Tuncel and R. Pöttgen  
**Page 948**



Temperature and field dependences of the magnetic entropy change for  $\text{Gd}_4\text{Co}_2\text{Mg}_3$  deduced from the magnetization measurements.  $\Delta S_{\text{M,F} \rightarrow \text{AF}}^{\text{PEAK}}$  and  $\Delta S_{\text{M,P} \rightarrow \text{F}}^{\text{PEAK}}$  denote the peak entropy changes, respectively, for the ferromagnetic to antiferromagnetic metamagnetic transition and for the paramagnetic to ferromagnetic ordering transition.

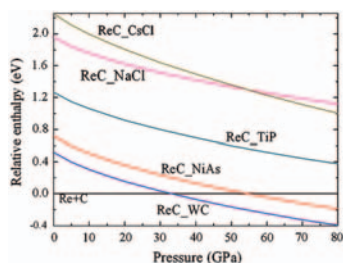
*Continued*

**Structural characterisation of the perovskite series  $\text{Sr}_{0.9-x}\text{Ca}_x\text{Ce}_{0.1}\text{MnO}_3$ : Influence of the Jahn–Teller effect**  
 Brendan J. Kennedy, Jimmy Ting, Qingdi Zhou, Zhaoming Zhang, Motohide Matsuda and Michihiro Miyake  
 Page 954



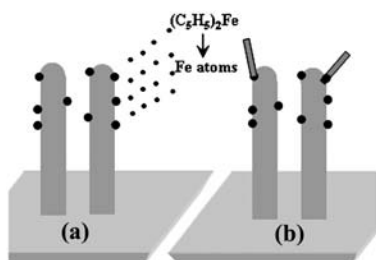
At room temperature the oxides with  $x \leq 0.45$  in the series  $\text{Sr}_{0.9-x}\text{Ca}_x\text{Ce}_{0.1}\text{MnO}_3$  are tetragonal in  $I4/mcm$  with a large Jahn–Teller distortion, and those with  $x \geq 0.55$  are orthorhombic, in  $Pbmm$ . Heating the tetragonal samples results in two transitions, ultimately the structure becomes cubic.

**Ab initio study on the electronic and mechanical properties of ReB and ReC**  
 Erjun Zhao, Jinping Wang, Jian Meng and Zhijian Wu  
 Page 960



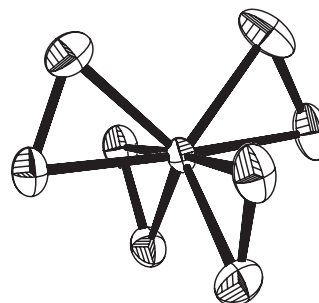
The enthalpy-pressure diagram for ReC from the selected structures. ReC–WC and ReC–NiAs become thermodynamically stable above 35 and 55 GPa, respectively. ReC–WC is the most stable phase.

**Two types of carbon nanocomposites: Graphite encapsulated iron nanoparticles and thin carbon nanotubes supported on thick carbon nanotubes, synthesized using PECVD**  
 Guangmin Yang, Xin Wang, Qiang Xu, Shumin Wang, Hongwei Tian and Weitao Zheng  
 Page 966



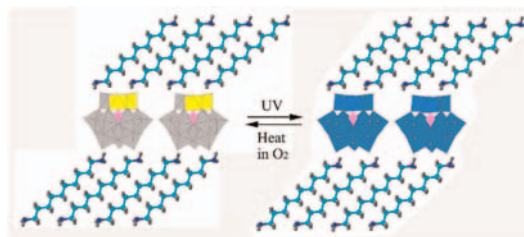
Graphite encapsulated Fe nanoparticles and thin carbon nanotubes supported on the pristine carbon nanotubes, respectively, were synthesized using plasma enhanced chemical vapor deposition.

**Structural investigation of tetraperoxo complexes of Mo(VI) and W(VI) X-ray and theoretical studies**  
 M. Grzywa, W. Łasocha and D. Rutkowska-Żbik  
 Page 973



Tetraperoxo compounds of Mo(VI) or W(VI) or V(V) have been obtained. Its crystal structures from single-crystal and from powder X-ray diffraction data have been determined. The compounds were characterised by IR spectroscopy and analytical methods. By means of the density functional theory (DFT) method, the geometry and stability of tetraperoxo complexes have been studied.

**Fabrication of self-assembled ultrathin photochromic films containing mixed-addenda polyoxometalates  $\text{H}_5[\text{PMo}_{10}\text{V}_2\text{O}_{40}]$  and 1,10-decanediamine**  
 Zhongliang Wang, Ying Ma, Ruili Zhang, Da Xu, Hongbing Fu and Jiannian Yao  
 Page 983



An ordered  $\text{H}_5[\text{PMo}_{10}\text{V}_2\text{O}_{40}]/1,10\text{-decanediamine}$  ultrathin film was fabricated by a self-assembled technique. The hybrid film displays good photochromism closely related to the reduction potentials of addenda atoms.

**Corrigendum**

Corrigendum to “Energy transfer and heat-treatment effect of photoluminescence in  $\text{Eu}^{3+}$ -doped  $\text{TbPO}_4$  nanowires” [Journal of Solid State Chemistry 180 (2007) 467–473]  
 Weihua Di, Xiaojun Wang, Peifeng Zhu and Baojiu Chen  
 Page 989

### **Author inquiries**

For inquiries relating to the submission of articles (including electronic submission where available) please visit this journal's homepage at <http://www.elsevier.com/locate/jssc>. You can track accepted articles at <http://www.elsevier.com/trackarticle> and set up e-mail alerts to inform you of when an article's status has changed. Also accessible from here is information on copyright, frequently asked questions and more.

Contact details for questions arising after acceptance of an article, especially those relating to proofs, will be provided by the publisher.

**Language services.** Authors who require information about language editing and copyediting services pre- and post-submission please visit <http://www.elsevier.com/locate/languagepolishing> or our customer support site at <http://epsupport.elsevier.com>. Please note Elsevier neither endorses nor takes responsibility for any products, goods or services offered by outside vendors through our services or in any advertising. For more information please refer to our Terms & Conditions <http://www.elsevier.com/termsandconditions>

For a full and complete Guide for Authors, please go to: <http://www.elsevier.com/locate/jssc>

*Journal of Solid State Chemistry* has no page charges.